ELSEVIER

Contents lists available at ScienceDirect

Earth and Planetary Science Letters

www.elsevier.com/locate/epsl



Precise determination of Ar, Kr and Xe isotopic fractionation due to diffusion and dissolution in fresh water



Alan M. Seltzer*, Jessica Ng, Jeffrey P. Severinghaus

Scripps Institution of Oceanography, La Jolla, CA, United States

ARTICLE INFO

Article history:
Received 30 October 2018
Received in revised form 1 March 2019
Accepted 6 March 2019
Available online xxxx
Editor: F. Moynier

Keywords: noble gas groundwater gas exchange isotope hydrology fractionation isotope geochemistry

ABSTRACT

Dissolved noble gases are ideal conservative tracers of physical processes in the Earth system due to their chemical and biological inertness. Although bulk concentrations of dissolved Ar, Kr, and Xe are commonly measured to constrain physical models of atmosphere, ocean, and terrestrial hydrosphere processes. stable isotope ratios of these gases (e.g. ¹³⁶Xe/¹²⁹Xe) are seldom used because of low signal-to-noise ratios. Here we present the first results from a new method of dissolved gas sampling, extraction and analysis that permits measurement of stable Ar, Kr, and Xe isotope ratios at or below \sim 5 per meg amu $^{-1}$ precision (1σ) , two orders-of-magnitude below conventional Kr and Xe isotopic measurements. This gain in precision was achieved by quantitative extraction and subsequent purification of dissolved noble gases from 2-L water samples via helium sparging and viscous dual-inlet isotope ratio mass spectrometry. We have determined the solubility fractionation factors (α_{sol}) for stable Ar, Kr, and Xe isotope ratios between $\sim\!\!2$ and $20\,^\circ\text{C}$ via laboratory equilibration experiments. We have also conducted temperaturecontrolled air-water gas exchange experiments to estimate the kinetic fractionation factors (α_{kin}) of these isotope ratios. We find that both α_{sol} and α_{kin} , normalized by isotopic mass difference (Δm), decrease in magnitude with atomic number but are proportional to Δm for isotope ratios of the same element. With the new ability for high precision isotopic measurements, we suggest that dissolved Kr and Xe isotope ratios in groundwater represent a promising, novel geochemical tool with important applications for groundwater modeling, water resource management, and paleoclimate.

© 2019 Elsevier B.V. All rights reserved.

1. Introduction

Because of their chemical and biological inertness, dissolved noble gases are widely used as quantitative geochemical tracers of physical processes in seawater and groundwater (Aeschbach-Hertig and Solomon, 2013; Stanley and Jenkins, 2013). Bulk dissolved noble gas concentrations - rather than isotope ratios - are frequently studied to constrain physical processes in the atmosphere, ocean, and terrestrial hydrosphere. Exceptions include dissolved helium isotope ratios, which exhibit large variations in nature (e.g. Jenkins et al., 1972; Torgersen and Clarke, 1985), and radiogenic and fissiogenic noble gas isotope ratios in extremely old (>1 Ma) groundwater (e.g. Lippmann et al., 2003). Common applications of dissolved noble gas measurements include quantifying groundwater recharge temperatures (e.g. Aeschbach-Hertig et al., 2000; Mazor, 1972; Stute et al., 1995) and abiotic properties of air-sea gas exchange (Hamme and Severinghaus, 2007; Loose et al., 2016; Stanley and Jenkins, 2013). Among recent studies that have measured dissolved

* Corresponding author.

E-mail address: aseltzer@ucsd.edu (A.M. Seltzer).

Ar, Kr, and Xe isotope ratios in seawater or groundwater, typical analytical $1-\sigma$ precision is on the order of 1% (Stanley et al., 2009; Wen et al., 2016), with the exception of one single higher-precision study of seawater Ar isotope ratios (Nicholson et al., 2010).

Here we present results from a new sampling, extraction and analysis system for high-precision measurement of dissolved stable Ar, Kr, and Xe isotope ratios. Quantitative extraction of dissolved gases from large water samples collected in air-tight 2-L flasks was achieved by sparging with ultra-high purity helium. Dissolved gases were subsequently purified and measured via viscous dualinlet multicollector isotope ratio mass spectrometry. The observed order-0.01% precision of individual isotope ratio measurements across replicate samples analyzed via this method represents a two orders-of-magnitude improvement over existing analytical techniques. Using this 2-L water sample method, we have carried out air-water gas-exchange experiments to determine the kinetic fractionation factors of Ar, Kr, and Xe isotopes in fresh water. A separate set of experiments to determine solubility fractionation factors was also conducted, by measuring noble gas isotope ratios in both the dissolved and gas phases of an equilibrated closed system, using fresh water ranging from \sim 2 to 20 °C.

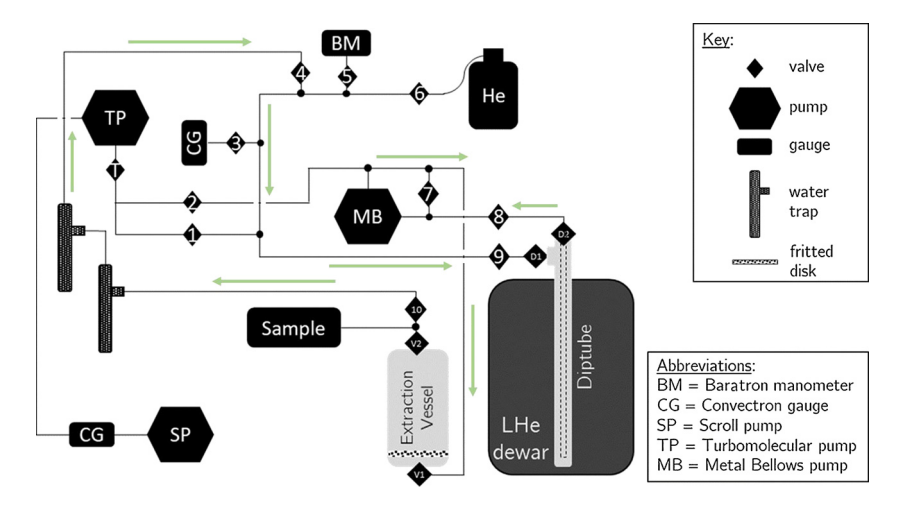


Fig. 1. Dissolved gas extraction system. Arrows indicate flow direction of liberated dissolved gases and helium carrier gas.

To our knowledge, these are the first solubility fractionation factor measurements of Kr and Xe isotope ratios in water. We discuss the sensitivity of observed solubility and kinetic fractionation factors to temperature and isotopic mass differences. We also compare our results to previous estimates of $^{40}/_{36}\mathrm{Ar}$ solubility and kinetic fractionation factors (Tempest and Emerson, 2013; Tyroller et al., 2014) and a recent study which found no fractionation (at order-1‰ precision) of Kr or Xe isotope ratios due to diffusion through water (Tyroller et al., 2018). Finally, we discuss the implications of our new findings for the potential of Kr and Xe isotope ratios in groundwater as quantitative indicators of past water-table depth.

2. Methods

2.1. Dissolved gas sampling, extraction, purification, and analysis

In this study, 2-L water samples were collected in evacuated glass flasks by a method similar to that of Hamme and Emerson (2004a). Custom glass flasks were used, fitted with two 9-mm Louwers-Hapert valves, each with two inner Viton o-rings separated by a \sim 0.04 cm³ space for sealing redundancy. To collect a sample, the neck of an evacuated flask was first inserted into \sim 25 cm of PVC tubing (\sim 1.25 cm inner diameter), forming an elongated neck. Next, ambient air inside the elongated neck was flushed out by inserting a thin nylon tube (0.25 cm inner diameter) carrying N₂ from a compressed gas cylinder. With N₂ flowing, a second thin nylon tube (0.25-0.5 cm inner diameter) was inserted carrying the water sample from either the laboratory equilibration bath or a groundwater well. With the elongated tube filled completely with water, the N₂ tube was removed and the flask valve was opened only enough to expose the inner o-ring to the water. This allowed any air in the cavity between the two o-rings to be flushed out. Care was taken to dislodge any bubbles. Once the elongated neck was free of bubbles, sample collection was begun by opening the valve to allow water to enter the flask. The valve position was adjusted throughout sampling to ensure that a roughly 20 cm column of water sat in the elongated neck between the valve and ambient air. Once \sim 95% full, the valve was closed leaving a small headspace to allow for any possible thermal expansion of the water during storage. The cavity between the two o-rings, and the space between the outer o-ring and a cap on the end of the neck, were flushed with N2 to minimize any possible permeation of atmospheric noble gases into the sample headspace during storage.

Dissolved gases were quantitatively extracted using a helium carrier-gas sparging system (Fig. 1). For each sample, water was first introduced to the evacuated system and poured into the extraction vessel. Any residual gas in the flask was then cryogenically transferred to a stainless-steel diptube immersed in liquid helium $(\sim 4 \text{ K})$ for 15 min, and then the sample flask (now evacuated) was closed to the system. Ultra-high purity tank helium was then introduced to the system, bringing the total pressure to \sim 1 atm before beginning a 90-min sparging. During the sparging period, a Metal Bellows MB-41 pump recirculated helium at $\sim 1 L_{STP} min^{-1}$, inducing bubbling through a fritted disc (with $\sim 10^{-4}$ m diameter pores) at the base of the extraction vessel and thereby stripping gases from solution. These liberated gases were then carried through two glass traps at -80 °C to remove water vapor before being trapped in the 4K diptube. The gaseous helium, which cannot be trapped in the diptube due to its low boiling point, continually circulated through the system during the 90-min extraction. To avoid adsorption saturation of the available surface area in the diptube, the tube was progressively lowered from \sim 15 cm above the liquid helium dewar to complete immersion over the sparging period.

At the end of the sparging period, residual helium was pumped to waste before closing the diptube and removing it from the liquid helium dewar. Trapped gases were warmed to room temperature and then exposed to SAES Zr/Al getter sheets and Ti sponge at \sim 900 °C for 125 min. To absorb any released H₂, the getter oven temperature was subsequently lowered to ~300°C for five minutes and then remaining noble gases were cryogenically trapped into a second diptube at 4K. After allowing at least three hours of homogenization at room temperature, the gettered gas sample pressure was measured in a calibrated volume attached to the inlet of a MAT 253 dual-inlet mass spectrometer in the Scripps Institution of Oceanography (SIO) Noble Gas Isotope Laboratory. The temperature of the volume was recorded to enable a subsequent manometric determination of dissolved Ar concentration. For each sample, Ar isotopes were analyzed first, followed by Xe isotopes and then Kr isotopes. During isotopic analyses of each separate gas, isotopes were measured by simultaneous collection, and Kr/Ar and Xe/Ar ratios via sequential, non-simultaneous peak jumping.

The measurements presented in this study were made as part of two wider analytical campaigns, which included measurements outside the scope of this study. The replacement of the ion source filament in mid-June 2018 separated campaign A (March-June 2018) from campaign B (June-October 2018). Because the replacement campaign-B filament had lower sensitivity than the original campaign-A filament, the ion beam intensities, integration times, and number of integration cycles were adjusted to achieve comparable precision. A summary of analytical parameters for each measurement campaign is presented in the supplemental materials (Supplemental Table S1). Each sample analyzed in both measure-

Table 1
Ar, Kr, and Xe isotopic solubility (at 15 °C) and kinetic fractionations (ε values) and measurement precision of campaigns A and B. ε and σ values have units of ‰, d ε _{sol}/dT has units of ‰ °C⁻¹, and Δ m has units of amu.

	$\delta^{40}/_{36} Ar$	$\delta^{38}/_{36}$ Ar	$\delta^{86}/_{82} \mathrm{Kr}$	$\delta^{86}/_{83} \mathrm{Kr}$	$\delta^{86}/_{84} \mathrm{Kr}$	$\delta^{136}/_{129}$ Xe	$\delta^{134}/_{129}$ Xe	$\delta^{132}/_{129}$ Xe
Δm	4	2	4	3	2	7	5	3
$\sigma_{ m pld,A}$	0.019	0.021	0.017	0.015	0.012	0.031	0.028	0.019
$\sigma_{ m pld,B}$	0.019	0.012	0.024	0.027	0.023	0.046	0.051	0.029
$\varepsilon_{\mathrm{sol}}$	1.072	0.563	0.237	0.172	0.119	0.156	0.121	0.067
$d\varepsilon_{sol}/dT$	-0.007	-0.004	-0.001	0.000	-0.001	0.000	0.002	0.000
$\varepsilon_{ m kin}$	-3.689	-1.946	-1.384	-1.205	-0.769	-0.998	-0.564	-0.400

ment campaigns was measured against the same working standard (ST-AEW1).

2.2. Measurements, corrections, and reproducibility

For each dissolved gas sample, eight independent isotope ratios were measured in addition to Xe/Ar ratios, Kr/Ar ratios, and Ar concentrations (via manometry). Xe and Kr concentrations were subsequently determined by multiplying measured Xe/Ar and Kr/Ar ratios by Ar concentrations. All gas and isotope ratios are reported in units of %0 with respect to the well-mixed atmosphere:

$$\delta^h/l \equiv \left(\frac{(h/l)_{\text{meas}}}{(h/l)_{\text{atm}}} - 1\right) 10^3 \tag{1}$$

where *h* and *l* refer to heavy and light gases or isotopes, respectively. Atmospheric air, routinely collected from the end of the research pier at SIO, was analyzed relative to working standard ST-AEW1 throughout the measurement campaigns. For Kr and Xe isotope measurements, aliquots of ST-AEW1 were mixed with pure Ar to match the Kr/Ar and Xe/Ar ratios of atmospheric air. This served two important purposes: first, it minimized chemical slope corrections (Severinghaus et al., 2003) in these measurements; second, it ensured that the run pressures in both the sample and standard bellows of the mass spectrometer were equal (whereas the pressures would differ by a factor of three for Xe isotope measurements of pure air vs ST-AEW1).

We report the precision of measured isotope ratios as pooled standard deviations of replicate samples, $\sigma_{\rm pld}$, from the mean of replicates from the same source. That is, for n total replicate samples collected from k distinct water sources (e.g. equilibration experiments, groundwater wells):

$$\sigma_{\text{pld}} \equiv \sqrt{\frac{\sum_{i,j=1}^{n,k} (\delta_i - \overline{\delta}_j)^2}{n-k}}$$
 (2)

 $\sigma_{\rm pld}$ values for individual measured isotope ratios during each campaign are presented in Table 1 and Fig. 2.

To minimize redundancy in the presentation of measured Xe and Kr isotope ratios, we make use of the nearly linear mass proportionality of Kr and Xe isotopic fractionation, following Orsi (2013), to define the following mass difference-normalized, error-weighted mean variables (in units of per meg amu⁻¹):

$$\delta^* \text{Kr} \equiv \left(\frac{\frac{\delta^{86}/82 \text{Kr}}{\sigma_{86/82}^2} + \frac{\delta^{86}/83 \text{Kr}}{\sigma_{86/83}^2} + \frac{\delta^{86}/84 \text{Kr}}{\sigma_{86/84}^2}}{\frac{4}{\sigma_{86/82}^2} + \frac{3}{\sigma_{86/83}^2} + \frac{2}{\sigma_{86/84}^2}}\right) 10^3$$
(3)

$$\delta^* Xe \equiv \left(\frac{\frac{\delta^{136}/_{129} Xe}{\sigma_{136/129}^2} + \frac{\delta^{134}/_{129} Xe}{\sigma_{134/129}^2} + \frac{\delta^{132}/_{129} Xe}{\sigma_{132/129}^2}}{\frac{7}{\sigma_{136/129}^2} + \frac{5}{\sigma_{134/129}^2} + \frac{3}{\sigma_{132/129}^2}} \right) 10^3$$
 (4)

The observed linear mass proportionality in our solubility and kinetic fractionation factors of Kr and Xe isotopes in water (Fig. 7,

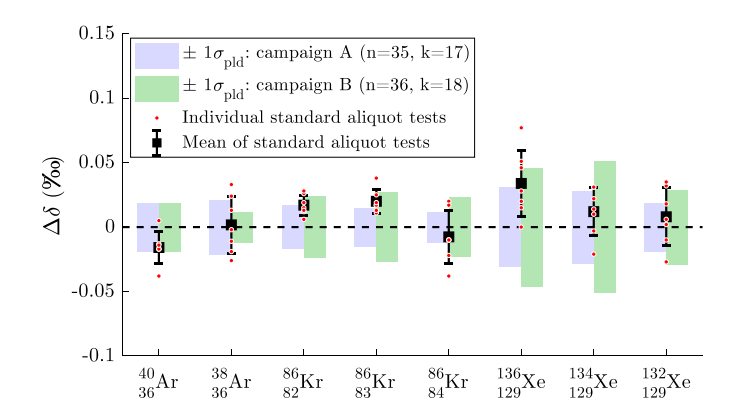


Fig. 2. Reproducibility of isotope ratio measurements, expressed as pooled standard deviations, and results of repeat standard aliquot tests. Standard aliquot test values are reported as isotope ratio departures, $\Delta\delta$, from the known composition of the reference gas used in the tests (ST-AEW2). (For interpretation of the colors in the figure(s), the reader is referred to the web version of this article.)

Section 4.1) further justifies the use of $\delta^* \text{Kr}$ and $\delta^* \text{Xe}$. The precision (σ_{pld}) of $\delta^* \text{Kr}$ and $\delta^* \text{Xe}$ was 2.9 and 3.2 per meg amu $^{-1}$, respectively, during campaign A and 5.3 and 5.2 per meg amu $^{-1}$, respectively, during campaign B.

Ar concentrations were determined manometrically, correcting for the contribution of Ne in air-equilibrated water (<0.1% of total gas pressure) and non-ideality of Ar gas using the first Virial coefficient. Measured Ar concentrations were then corrected for incompleteness of extractions. Mean Ar extraction efficiency was determined to be 99.7 \pm 0.1% based on four repeat experiments in which $^{40}\mathrm{Ar}$ ion beam intensities were compared between dissolved gas samples and residual gases, which were subsequently extracted and processed identically.

Three separate small corrections, on the order of σ_{pld} , were made to measured isotope ratios for 1) the so-called "chemical slope" (the influence of Ar concentration differences between the sample and reference aliquots on Xe and Kr isotope ratios (Severinghaus et al., 2003)), 2) the sensitivity of measured Ar, Kr, and Xe isotope ratios to total pressure imbalances between sample and reference gas (Severinghaus et al., 2003), and 3) trace amounts of "apparent fractionation" by the dissolved gas extraction and/or purification methods, as follows.

To empirically estimate the apparent fractionation of individual Ar, Kr, and Xe isotope ratios due to extraction and/or purification, we carried out seven repeat experiments (hereafter "standard aliquot tests"). During each standard aliquot test, an aliquot of gas from working standard can ST-AEW2 was introduced to the extraction vessel, which was prepared with two liters of >99.9% degassed water (except for helium). The extraction and purification method were then carried out in an identical manner to an actual water sample. For each standard aliquot test, measured isotope ratios (versus ST-AEW2) were normalized to the mean of 18 measurements of ST-AEW2 vs ST-AEW1 carried out over the course of campaign A. In other words, an observed deviation of 0% from the known ST-AEW2 value would imply that there was no frac-

tionation of the standard gas aliquot due to the extraction and purification methods.

For each measured isotope ratio, corrections were made to dissolved gas samples equal to the magnitudes of mean apparent fractionation across all standard aliquot tests (black squares in Fig. 2), which in all cases were below campaign B $\sigma_{\rm pld}$ values. Although these corrections are sufficiently small to ensure confidence in the data presented in this study, their non-zero values suggest scope for future improvement of the method. We speculate that they may reflect two processes: slight kinetic fractionation associated with the order 0.1% incompleteness of extractions, and isobaric interference by substances resistant to Zr/Al and Ti gettering.

2.3. Solubility fractionation experiments

To determine the solubility fractionation factors (α_{sol}) of Ar, Kr, and Xe isotopes in fresh water at temperatures between \sim 2 and 20 °C, we conducted both closed-system (CS) and open-air (OA) equilibration experiments. These experiments are described in detail in Sections 2.3.1 and 2.3.2. Solubility fractionation factors, α_{sol} , are defined for an isotope ratio R as:

$$\alpha_{\rm sol} \equiv \frac{R_{\rm diss}}{R_{\rm gas}} \tag{5}$$

where $R_{\rm gas}$ and $R_{\rm diss}$ refer respectively to isotope ratio R in the gas and dissolved phases at equilibrium. Throughout the text, we often refer to ε values where $\varepsilon \equiv \alpha - 1$ (in units of ‰, per meg, or per meg amu⁻¹, if normalized by isotopic mass difference).

In individual OA experiments, 2-L water samples were collected from an isothermal bath of de-ionized (DI) water after 4–14 days of gas-exchange with laboratory air. In each sample, Ar, Kr, and Xe isotope ratios were analyzed and compared against atmospheric air. In CS experiments, an initially degassed reservoir of DI water was equilibrated with a pure noble gas headspace in a closed system surrounded by an isothermal water bath. At the end of each experiment, isotope ratios of a specific gas (Ar, Kr, or Xe) were analyzed both in the water and headspace.

The CS experiments – in which pressure, temperature, and humidity were constant throughout the equilibrating headspace – revealed that the OA experiments exhibited reproducible temperature-dependent biases, which were most significant for Ar isotopes at cold temperatures. We suggest that these biases were due to thermal diffusion (Grew and Ibbs, 1953) and water-vapor flux fractionation (Severinghaus et al., 1996) caused by gradients in temperature and absolute humidity between well-mixed atmospheric air in the laboratory and a thin stagnant air layer (hereafter SAL) above the water bath. A physical model for observed OA-CS differences is presented and discussed in Supplemental Section S1. Due to the discovery of the SAL fractionation in the OA experiments, our determinations of $\varepsilon_{\rm SOI}$ (Section 3.1) are based solely on the CS experiments.

2.3.1. Description of CS equilibration experiments

CS experiments were carried out by bringing \sim 200–300 cm³ of initially degassed water to solubility equilibrium with a \sim 1.8 L headspace, filled with pure Ar, Kr and Xe at \sim 1 atm total pressure inside a closed \sim 2-L chamber at constant temperature (Supplemental Fig. S1). Each equilibration was carried out for at least 36 h, during which the water reservoir was continuously stirred by a magnetic stirrer at 500 revolutions per minute. Upon completion of the experiment, a 2 cm³ sample of headspace gas and a \sim 10 cm³ sample of water were collected simultaneously. The headspace samples were collected in an aliquot chamber connected to the headspace throughout the duration of each experiment. Water samples were collected in a \sim 40 cm³ glass volume

evacuated immediately prior to sample collection. Dissolved gases were extracted from water samples under vacuum, using a magnetic stirrer to accelerate degassing, and collected in a stainless-steel dip tube immersed in liquid helium downstream of a $-80\,^{\circ}\text{C}$ water trap. Extracted gas and headspace gas samples were gettered using SAES Zr/Al sheets for 90 min (for Ar isotope samples) and 60 min (for Kr and Xe isotope samples) at 900 °C. Purified headspace and dissolved gas samples were then measured on a MAT 253 mass spectrometer against a common reference gas (ST-AEW1). The measured δ values of the headspace and dissolved gas samples, $\delta_{\rm hs}$ and $\delta_{\rm diss}$, respectively, were used to calculate $\alpha_{\rm sol}$:

$$\alpha_{\text{sol}} = \frac{\frac{\delta_{\text{diss}}}{1000} + 1}{\frac{\delta_{\text{hs}}}{1000} + 1} \tag{6}$$

where δ_{hs} and δ_{diss} are reported with respect to the same reference gas.

In total, 18 individual CS experiments were carried out: seven Ar isotope experiments, six Kr isotope experiments, and five Xe isotope experiments. In each Kr and Xe experiment, Kr/Ar and Xe/Ar ratios in the headspace were both $\sim 10^{-3}$, roughly ten and one hundred times larger than their respective atmospheric ratios. Isotopes of different gases could not be measured in the same experiments because pure Ar gas was added, in different proportions, to the dissolved gas samples for each Kr and Xe isotope experiment. The purpose of adding Ar was to ensure that Kr/Ar or Xe/Ar ratios were the same between headspace and dissolved gas samples. Ensuring constant Kr/Ar or Xe/Ar between headspace and dissolved samples fulfilled two important needs: 1) given the large solubility differences between Kr, Xe, and Ar, it allowed for the total gas pressure (mostly Ar) to be sufficiently high to ensure viscous flow during analysis, and 2) it circumvented the need for any chemical slope corrections (described in Section 2.2 for 2-L water samples). Because the equilibration temperature for each experiment was known, exact Ar concentrations could be added to dissolved gas samples based on the known solubility ratios of Kr, Xe and Ar in fresh water (Clever, 1979; Hamme and Emerson, 2004b).

Throughout each experiment, an Arduino microprocessor logged water temperatures at the top and bottom of the equilibration bath, as well as air temperature, humidity, and pressure just above the surface of the bath at \sim 2.5-min intervals. Observations and a simple model both indicated that isotopic equilibration was achieved after 36 h and that a 30-min extraction time allowed for quantitative extraction of all dissolved gases (Supplemental Figs. 4 and 5). For Ar isotopes, which have the largest-magnitude kinetic and solubility fractionation factors of the isotope ratios considered in this study (Sections 3.1 and 3.2), individual experiment anomalies of $\varepsilon_{\rm sol}$ from a linear trendline of $\varepsilon_{\rm sol}$ vs temperature revealed no dependence on equilibration time (between 1.5 and 2.5 days) or extraction time (between 30 and 55 min). In a simple twobox diffusive gas exchange model, we simulated the equilibration of 300 cm³ of degassed water with a 1.8-L pure Ar headspace at 1 atm initial pressure and 2 °C. Numerical integration of this model at 0.5-min resolution suggested that 40 Ar/36 Ar would achieve solubility equilibrium (to within 1 per meg) within 1.3 days (Supplemental Fig. S4). This calculation used a conservatively low gas transfer velocity of 0.2 m day⁻¹ (over three times smaller than gas transfer velocities observed in the experiments described in Section 3.2) and assumed both the CS solubility fractionation factors and kinetic fractionation factors found in this study (Fig. 4). Because actual gas transfer velocities were likely much higher in CS experiments, we are confident that 36 h is sufficient to achieve isotopic solubility equilibrium.

2.3.2. Description of OA equilibration experiments

Each OA experiment involved gas-exchange between a \sim 15-L bath of DI water and atmospheric air in the SIO Noble Gas Isotope Laboratory. The water bath was maintained at constant temperature by a recirculating chiller and mixed continuously by an overhead stirrer (Supplemental Fig. S2). Because exchange of laboratory air with outside atmosphere air is rapid, with an overturning timescale of \sim 10 min, we assume noble gas concentrations and isotopic ratios in the laboratory are atmospheric and constant over time. Individual OA equilibration experiments were carried out for 4-14 days, after which 2-L samples were collected using the sampling method described in Section 2.1. Each 2-L OA sample was analyzed for Ar, Kr, and Xe isotope ratios in addition to bulk Ar, Kr and Xe concentrations. In the absence of any fractionation between atmospheric air in the laboratory and the SAL above the equilibration bath, measured isotope ratios from OA samples, divided by their ratios measured in atmospheric air, would be equal to α_{sol} . In total, 17 OA samples from 12 total experiments were analyzed (two outlier samples collected from a single equilibration experiment at 2 °C were rejected).

We originally neglected to consider the possibility of fractionation between atmospheric air in the lab and the SAL above the water bath, which equilibrates with dissolved gases in solution. However, as described in Supplemental Section 1, we observed small reproducible, temperature-dependent offsets between OA and CS-derived estimates of $\varepsilon_{\rm sol}$ (Supplemental Figs. S6 and S7). In light of these offsets, our ultimate determination of solubility fractionation factors is restricted to the results of the CS experiments. However, we used the differences between OA and CS experiments to estimate a temperature-dependent fractionation factor between the SAL and atmospheric air, $\alpha_{\rm SAL}$, and its uncertainty, which we explicitly account for in the model-based interpretation of the kinetic fractionation experiments.

2.4. Kinetic fractionation experiments

To determine kinetic isotopic fractionation factors ($\alpha_{\rm kin}$), we designed and carried out three nearly identical gas-exchange experiments using the same temperature-controlled water bath used for OA equilibration experiments. The fractionation factor $\alpha_{\rm kin}$ for diffusive gas exchange is defined by the ratio of heavy and light isotope piston velocities, k_h and k_l , respectively:

$$\alpha_{\rm kin} \equiv \frac{k_h}{k_l} \tag{7}$$

Each experiment was conducted by first bringing the water bath used in the OA equilibration experiments to steady state at $\sim\!13\,^\circ\text{C}$, then rapidly cooling the well-mixed bath over $\sim\!3$ h by $\sim\!10\,^\circ\text{C}$, and finally collecting two replicate 2-L water samples over a period of $\sim\!10$ min. These rapid cooling experiments (RCEs) induced rapid dissolution of atmospheric gases due to the increasing solubilities of Ar, Kr, and Xe in the cooling reservoir. By measuring bulk gas concentrations ([Ar], [Kr], and [Xe]) and isotope ratios in each sample and logging the water temperature and air pressure throughout each experiment, we were able to constrain a simple one-box diffusive model of gas exchange to numerically solve for $\alpha_{\rm kin}$. For each RCE, there were two stages of least-squares optimization required to arrive at a value and uncertainty range for $\alpha_{\rm kin}$ for each separate isotope ratio.

In the first stage, we used the MATLAB nonlinear solver *fminsearch* to seek initial piston velocities, $k_{g,0}$, for Ar, Kr, and Xe that minimized squared deviations between replicate-mean measured gas concentrations, and concentrations modeled by numerically integrating Equation (8) at 0.5 min resolution:

$$\frac{dC_g(t)}{dt} = \frac{1}{L} k_{g,0} \left(1 + \mu T(t) \right) \left(C_{g,eq} \left(T(t), P(t) \right) - C_g(t) \right) \tag{8}$$

In Equation (8) at time t (min), C_g is the dissolved concentration of gas g (mol cm⁻³), L is the depth of the water reservoir (cm), μ is the fractional change in piston velocity for a change in temperature (°C⁻¹) from a linear fit to the data of Jähne et al. (1987), T is the reservoir temperature at time t (°C), and $C_{g,eq}$ is the solubility concentration (mol cm⁻³) of gas g at temperature T and pressure P (Torr). For each integration of Equation (8), the histories of T and P throughout each experiment were prescribed from RCE observations. We carried out 1000 Monte Carlo simulations per experiment for each of the three gases (Ar, Kr, and Xe), adding Gaussian perturbations to the measured concentrations with standard deviations equal to the pooled measurement standard deviations and to the temperature history based on the absolute temperature uncertainty associated with the sensors.

In the second stage, having already solved for a distribution of $k_{g,0}$ values for Ar, Kr, and Xe in the first stage, we again used *fminsearch* for each individual Monte Carlo simulation, isotope ratio, and experiment to seek a value of $\alpha_{\rm kin}$ that minimized squared deviations between measured replicate-mean δ values and modeled experiment-end δ values (Equations (9)–(11)).

$$\frac{dC_{h}(t)}{dt} = \frac{1}{L} \alpha_{kin} k_{g,0} (1 + \mu T(t)) f_{h} (\alpha_{sol} \alpha_{SAL} C_{g,eq} (T(t), P(t)) - C_{g}(t))$$
(9)

$$\frac{dC_l(t)}{dt} = \frac{1}{L} k_{g,0} \left(1 + \mu T(t) \right) f_l \left(C_{g,eq} \left(T(t), P(t) \right) - C_g(t) \right) \tag{10}$$

$$\delta = \left(\frac{\frac{C_h}{C_l}}{\frac{f_h}{f_t}} - 1\right) 10^3 \tag{11}$$

In Equations (9) and (10) at time t, C_h and C_l are the dissolved concentrations of the heavy and light isotope, respectively, and f_h and f_l are the mole fractions of the heavy and light isotope, respectively, in atmospheric air. We account for the observed fractionation of noble gas isotope ratios in the stagnant air layer by including the empirically estimated fractionation factor (α_{SAL}), which represents heavy-to-light temperature-dependent isotopic fractionation between atmospheric air and the stagnant air layer (Supplemental Figs. S6 and S7) in Equation (9). As in the first stage, we conducted 1000 Monte Carlo simulations in which Gaussian perturbations were added to the measured isotope ratios, solubility fractionation factor (α_{sol}), and SAL fractionation factor (α_{SAL}) determined from differences in linear fits of CS and OA data to experiment temperatures. By comparing modeled δ values at the end of the simulated experiment to measured δ values, we generated probability distributions of α_{kin} each isotope ratio in each experi-

The equilibrium solubility concentrations, $C_{g,eq}$, and isotopic solubility ratios, α_{sol} , were prescribed from best fit curves based on the OA equilibration experiments described in section 2.3.2. By using the OA-experiment derived solubility curves, we eliminate any potential bias that could be introduced by using prior solubility curves in the literature that might not have accounted for the slight fractionation of the stagnant air layer. We note that our fitted OA-equilibration Ar, Kr, and Xe solubility curves agree well (within \sim 1% at all temperatures) with previously published Ar, Kr, and Xe solubility curves (Supplemental Fig. S11; Clever, 1979; Hamme and Emerson, 2004b).

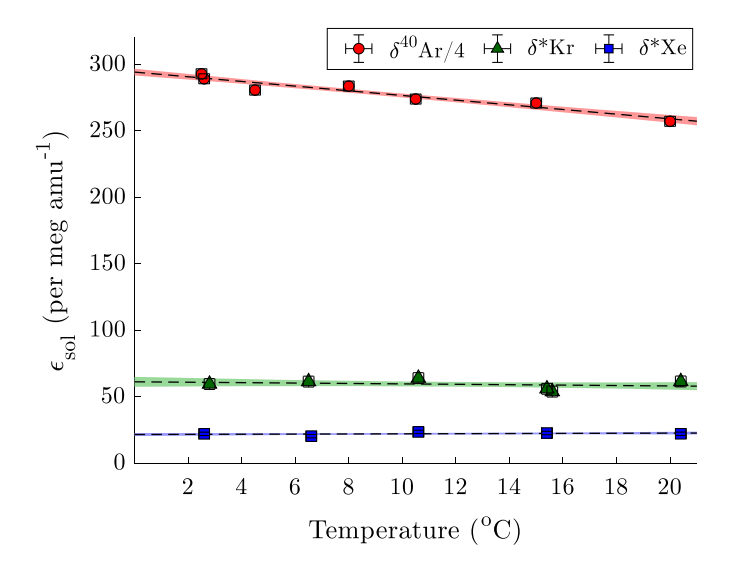


Fig. 3. Mass-normalized freshwater solubility $\varepsilon_{\rm Sol}$ values between \sim 2 and 20 °C determined in closed-system (CS) equilibration experiments. Markers represent values for individual experiments, each constrained by a pair of measurements (one dissolved gas and one headspace gas measurement) at solubility equilibrium. Vertical error bars indicate individual measurement precision ($\pm 1\sigma$), shaded error regions around dashed trendlines indicate $\pm 1-\sigma$ range of linear fits, and horizontal error bars indicate ± 0.2 °C absolute error of equilibration temperatures.

3. Results

3.1. Solubility fractionation factors

We present the mass-normalized $\varepsilon_{\rm sol}$ values for Ar, Kr, and Xe isotope ratios between ~2 and 20 °C from the 18 CS-equilibration experiments carried out in this study (Fig. 3). Table 1 provides the observed $\varepsilon_{\rm sol}$ values of individual isotope ratios (at 15 °C) and their temperature dependences. Normalized by isotopic mass difference, argon isotopes exhibit the strongest solubility fractionation, followed by krypton and then xenon isotopes, at all temperatures. Interestingly, only the temperature sensitivity of Ar isotopic solubility fractionation is statistically significant from zero. The regression coefficient of $\varepsilon_{\rm sol}$ versus temperature for $^{40}{\rm Ar}/^{36}{\rm Ar}$ is -1.8per meg amu⁻¹ °C⁻¹ ($R^2 = 0.92$, p < < 0.05), whereas for Kr isotopes and Xe isotopes the coefficients are orders of magnitude smaller: -0.16 per meg amu $^{-1} \circ C^{-1}$ ($R^2 = 0.07$, p = 0.61) and 0.05 per meg amu⁻¹ ${}^{\circ}C^{-1}$ ($R^2 = 0.10$, p = 0.60), respectively. We estimate the 1- σ precision of individual CS experiments as the standard deviation of individual experiment ε_{sol} values from the linear temperature trendlines, which indicate Ar, Kr, and Xe isotopic precisions of 3.0 per amu⁻¹, 4.1 per meg amu⁻¹, and 1.3 per $meg amu^{-1}$, respectively.

The observed positive sign of $\varepsilon_{\rm sol}$ for all isotope ratios measured in this study is typical for monatomic and diatomic gas heavy-to-light isotope ratios (Benson and Krause, 1984, 1980; Klots and Benson, 1963; Knox et al., 1992; Muccitelli and Wen, 1978; Tempest and Emerson, 2013). Supplemental Fig. S12 also shows observed temperature-dependent $\varepsilon_{\rm sol}$ values for $\delta^{38}/_{36}{\rm Ar}$ (from this study) alongside experimental values from the literature for noble gas, O₂, and N₂ stable isotope ratios. At 20 °C, we find that $\varepsilon_{\rm sol}$ for $\delta^{40}/_{36}{\rm Ar}$ is $1.036\pm0.012\%$, agreeing reasonably well with Tempest and Emerson (2013) who found $1.07\pm0.02\%$ at the same temperature. Our results are also broadly consistent with a lower resolution compilation of 70 surface freshwater $\delta^{40}/_{36}{\rm Ar}$ isotope measurements, which found a mean value of $1.3\pm0.2\%$ (Beyerle et al., 2000). We know of no prior studies in which Kr or Xe isotopic solubility fractionation has been measured.

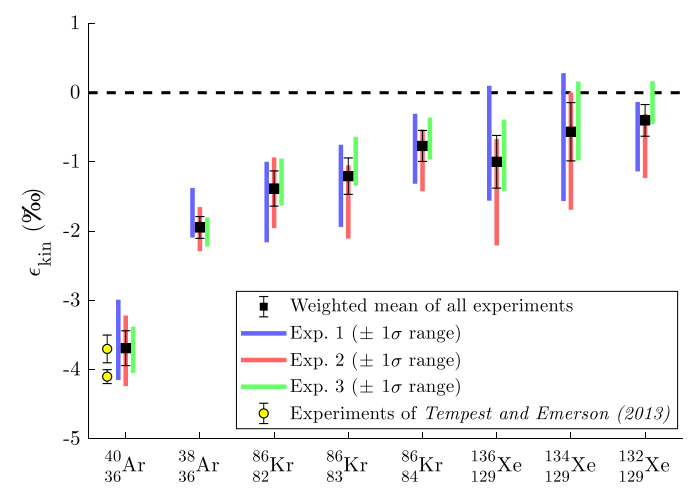


Fig. 4. Weighted-mean $\varepsilon_{\rm kin}$ values for each isotope ratio measured across three rapid cooling experiments. Colored bars represent ± 1 - σ confidence ranges from three individual experiments (from least-squares fits of 1000 Monte Carlo simulations to observations for each experiment and isotope ratio). Yellow circles indicate results of two 40 Ar/ 36 Ar kinetic fractionation experiments presented in Tempest and Emerson (2013) using an independent experimental method.

3.2. Kinetic fractionation factors

In all three rapid cooling experiments, each replicate-mean measured heavy-to-light isotope ratio decreased over time from its initial OA experiment steady-state value at $\sim\!13\,^\circ\text{C}$, consistent with the canonical viewpoint that heavy isotopes diffuse more slowly than light isotopes. Bulk Ar, Kr, and Xe concentrations all increased as expected, indicating rapid gas uptake induced by cooling. The isotopic kinetic fractionation factors ($\varepsilon_{\rm kin}$ values) determined in these RCEs are shown in Fig. 4 and Table 1. Weighted-mean $\alpha_{\rm kin}$ values, calculated for each isotope ratio based on probability distributions resulting from 1000 Monte Carlo simulations for each RCE, were below unity in all cases. That is, for each measured isotope ratio in each experiment, we observed the lighter isotope to have a faster piston velocity than then heavier isotope.

To provide a visual illustration of the two data-model optimization stages required for the determination of α_{kin} , we show specific results from a single experiment (RCE1) in Figs. 5 and 6. Fig. 5 shows 1000 modeled simulations of Ar, Kr, and Xe concentrations over ~180 min, a period in which 12.9 °C water, brought to steady state in an OA experiment, was rapidly cooled by $\sim 10 \, ^{\circ}$ C. As the water cooled, atmospheric Ar, Kr, and Xe were taken up resulting in measured \sim 5%, 6%, and 7% respective increases in concentration (relative to air-equilibrated 12.9 °C fresh water). The median initial piston velocities resulting from the 1000 Monte Carlo simulations were ~ 0.73 , ~ 0.66 , and ~ 0.66 m day⁻¹ for Ar, Kr, and Xe, respectively. α_{kin} values for each isotope ratio were then simulated by prescribing these distributions of initial piston velocities to numerically integrate Equations (9) and (10). Modeled Ar isotope histories, measured Ar isotopic fractionation, and probability distributions of resulting kinetic fractionation factors are shown (Fig. 6). Experiment-specific results for each RCE are included in the Supplemental materials (Supplemental Figs. S8-S10).

We note that because the total gas added in these RCEs to the pre-existing Ar, Kr, and Xe in solution was only \sim 5–10%, and calculated $\varepsilon_{\rm kin}$ values were on the order of 1‰, the total observed fractionation (order 0.01–0.1‰) provided a relatively low signal-to-noise ratio. For this reason, the probability distributions for $\varepsilon_{\rm kin}$ values (Figs. 4 and 6) span a range of order 0.1‰, considerably higher than $\sigma_{\rm pld}$ for any individual isotope ratio measured in this study. The values and uncertainty ranges for $\varepsilon_{\rm kin}$ found in this study are still useful for environmental tracer applications in

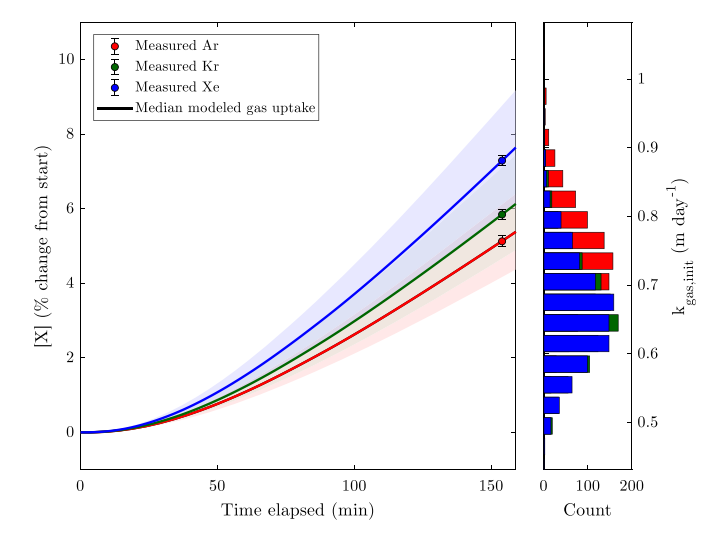


Fig. 5. Modeled evolutions of Ar, Kr, and Xe gas concentrations ([X]) during RCE1, in which a water-bath brought to steady state in an OA experiment at $12.9\,^{\circ}$ C over four days was cooled by $\sim \! 10\,^{\circ}$ C over $\sim \! 3$ h. In the left panel, markers indicate replicate-mean measured [Ar], [Kr], and [Xe] (filled circles) and solid lines indicate median modeled gas uptake by fitted gas exchange model (shaded regions indicate 95% confidence intervals of 1000 Monte Carlo simulations per gas). In the right panel, histograms of modeled Ar, Kr, and Xe piston velocities (at start of experiment) are shown from 1000 Monte Carlo gas-exchange model-data fits (described in Section 2.4). Measured and modeled concentrations are presented as percent departures from initial steady-state OA experiment conditions for $12.9\,^{\circ}$ C water.

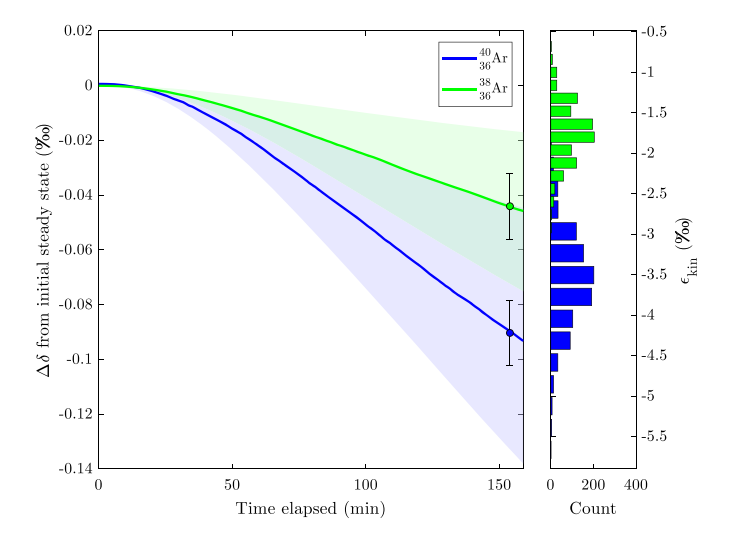


Fig. 6. Modeled $\delta^{40}/_{36}$ Ar and $\delta^{38}/_{36}$ Ar departures over the course of RCE1 from values in steady-state OA experiments at 12.9 °C. Shaded regions indicate 95% confidence intervals of 1000 Monte Carlo simulations (per isotope ratio) and filled circles show replicate-mean replicate values with ± 1 - σ uncertainty. Distributions of $\varepsilon_{\rm kin}$ values shown in right panel reflect least-squares minimization of measured data to 1000 Monte Carlo simulations.

groundwater and seawater (section 4.2) but could be resolved at even higher precision by conducting diffusion experiments with pure Ar, Kr, and Xe gas.

4. Discussion

4.1. Solubility and kinetic fractionation factors: comparison with past estimates, mass proportionality

The freshwater solubility fractionation factors presented in this study for Kr and Xe stable isotope ratios and $\delta^{38}/_{36}$ Ar are, to our knowledge, the first ever published. However, prior experiments have measured the solubility fractionation factor for $\delta^{40}/_{36}$ Ar at 20 °C (Tempest and Emerson, 2013) and the kinetic fractionation

factors for $\delta^{40}/_{36}$ Ar (Tempest and Emerson, 2013; Tyroller et al., 2014) and stable Kr and Xe isotopes (Tyroller et al., 2018). Our finding of $-3.69 \pm 0.25\%$ for the kinetic fractionation factor ($\varepsilon_{\rm kin}$) of $^{40}/_{36}$ Ar agrees reasonably well with Tempest and Emerson (2013), who found values of -3.7% and -4.1% in two closed-system gas exchange experiments (Fig. 4).

An unpublished freshwater ε_{sol} finding at 2 $^{\circ}\text{C}$ of 1.21% for $^{40}/_{36}$ Ar was referenced in Nicholson et al. (2010), who used this value to interpret deep-ocean $\delta^{40}/_{36}$ Ar solubility anomalies as constraints on ventilation of the deep ocean. The value obtained in our study at \sim 2 °C (1.163 \pm 0.009‰) is slightly lower. Because Nicholson et al. (2010) observed deep-ocean $\delta^{40}/_{36}$ Ar solubility anomalies on the order of 0.1%, this difference may affect physical interpretation of these disequilibria. We suggest that future measurements of deep-ocean $\delta^{40}/_{36} Ar$ and careful measurements of the solubility fractionation factor in seawater would be helpful in quantifying deep-ocean $\delta^{40}/_{36}$ Ar disequilibrium. Additionally, we believe that our finding of Kr and Xe $\varepsilon_{\mathrm{sol}}$ values that are small and (within error) insensitive to temperature (Fig. 3) has potential relevance to seawater applications. We suggest that Kr and Xe isotope ratios in the deep ocean may provide further constraints on kinetic fractionation during deep-water formation, since they should be rather insensitive to disequilibrium cooling and bubble injec-

We also compare our ε_{kin} estimates to prior studies which measured the diffusivity ratios of Ar, Kr, and Xe isotopes in water (Tyroller et al., 2018, 2014) by assuming that diffusivity ratios raised to the 2/3 power (Jähne et al., 1984; Ledwell, 1984) are equal to piston-velocity ratios for diffusive gas exchange across smooth interfaces. Tyroller et al. (2014) found an isotopic diffusivity ratio in water of 1.055 \pm 0.004 for $^{36}/_{40}$ Ar, equivalent to an $\varepsilon_{\rm kin}$ value of $\sim -35 \pm 3\%$ for $^{40}/_{36}$ Ar (for exchange across a smooth interface). This value is clearly inconsistent both with our result and the independent finding of Tempest and Emerson (2013). Tyroller et al. (2018) conclude that Kr and Xe isotope kinetic fractionation in water is negligible, finding diffusivity ratios of unity within their measurement precision. However, the stated measurement precision of Tyroller et al. (2018) is equivalent to $\sim \pm 1\%$, which is the order of the Kr and Xe $\varepsilon_{\rm kin}$ values found in this study. We suggest that kinetic fractionation of Kr and Xe isotopes in water, though small, is in fact not negligible at our level of precision. In fact, mass-proportional differences among different isotope ratios of Kr and Xe are even discernable (Fig. 7). We further suggest that higher-precision $\varepsilon_{\rm kin}$ estimates could be achieved by merging our dual-inlet mass spectrometry technique with a Barrer diffusion-cell experiment method (e.g. Tyroller et al., 2018, 2014).

Measured kinetic and solubility ε values (at 15 °C) are shown versus isotopic mass differences (Fig. 7). We find that the magnitude of both solubility and kinetic fractionation, for Kr and Xe isotopes, increases linearly with isotopic mass difference. Extended regression lines of the presented data pass through the origin within measurement precision. The apparent linear mass dependences of Kr and Xe isotope fractionation due to dissolution and diffusive gas exchange justify the use of δ^* Kr (Equation (3)) and δ^* Xe (Equation (4)) for dissolved gas measurements. The observed Ar isotopic solubility and kinetic fractionation factors also increase in magnitude with isotopic mass difference, but the relationship does not appear to be exactly linear (e.g. the ratio of $^{40}/_{36}$ Ar and $^{38}/_{36}$ Ar ε_{sol} values is slightly below 2, the ratio of their isotopic mass differences; Table 1, Supplemental Fig. S12). Overall, our observations are consistent with the conclusions of other recent noble gas isotope studies in water (Bourg and Sposito, 2008; Tempest and Emerson, 2013: Tyroller et al., 2018, 2014), which all found that the kinetic-theory expectation of a uniform square-root relationship between mass and diffusivity ratios fails to account

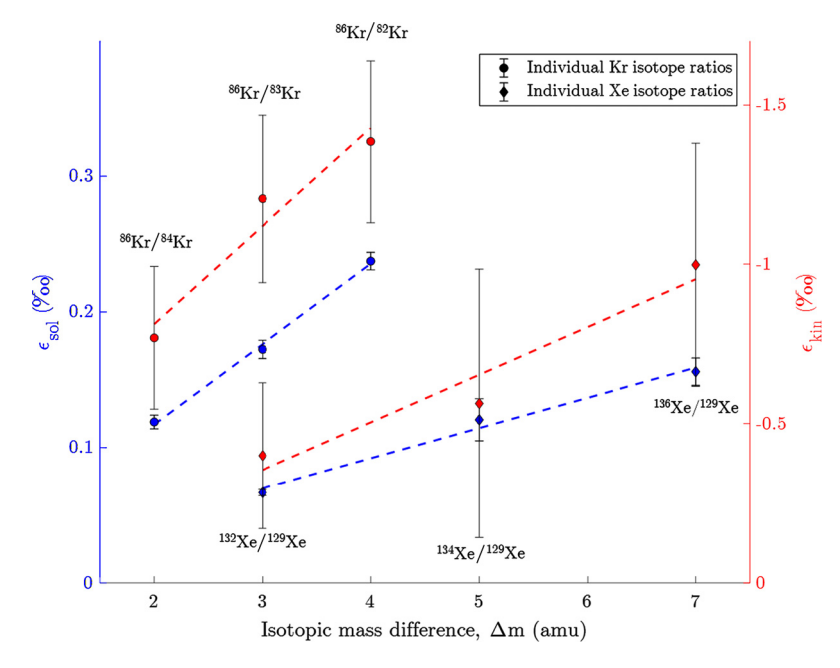


Fig. 7. Individual isotope ratio $ε_{sol}$ and $ε_{kin}$ values versus isotopic mass difference Δm for stable isotope ratios of Kr and Xe. The $ε_{sol}$ vs. Δm linear regression coefficients and intercepts, respectively, are 0.059% amu⁻¹ and -0.001% for Kr isotope ratios and 0.022% amu⁻¹ and 0.003% for Xe isotope ratios. The $ε_{kin}$ vs. Δm linear regression coefficients and intercepts, respectively, are -0.307% amu⁻¹ and -0.197% for Kr isotope ratios and -0.150% amu⁻¹ and 0.094% for Xe isotope ratios. The intercepts for all four regression lines pass through the origin within ±1-σ uncertainty.

for both observed and modeled kinetic fractionation of noble gas isotopes in water.

4.2. Implications for heavy noble gas isotope ratios as geochemical tracers

The newly determined solubility and kinetic isotopic fractionation measurements presented in this study have implications for potential applications of dissolved Ar, Kr, and Xe isotopes as tracers of physical processes in the atmosphere, ocean, and terrestrial hydrosphere. Here we briefly consider one such application: δ^* Kr and δ^* Xe in groundwater as quantitative indicators of past water-table depth. Prior work has indicated that Kr and Xe isotopes in the unsaturated zone are fractionated from their ratios in the well-mixed troposphere by gravitational settling (Seltzer et al., 2017). The dissolution of unsaturated zone gases into groundwater at the water table should preserve this gravitational fractionation signal in the dissolved isotope ratios of Kr and Xe. Because gravitational fractionation is a nearly linear function of depth, quantitative reconstruction of past water-table depth may be possible by measuring dissolved δ^* Kr and δ^* Xe in ancient groundwater samples that have not experienced gas exchange since the time of recharge.

The finding of Kr and Xe isotopic fractionation factors near unity ($\varepsilon_{\rm sol}$ and $\varepsilon_{\rm kin}$ close to zero) implies that groundwater $\delta^*{\rm Kr}$ and $\delta^*{\rm Xe}$ should be extremely insensitive to the injection and fractionation of excess air, which is a confounding issue in noble-gas paleotemperature studies (e.g. Stute et al., 1995). To demonstrate the importance of this insensitivity, we assume that the isotopic composition of groundwater, $\delta_{\rm diss,\,gw}$, reflects the gravitationally-fractionated isotopic composition of unsaturated zone air above the water table, $\delta_{\rm UZ,\,WT}$, plus solubility fractionation and fractionation due to excess air:

$$\delta_{\text{diss.gw}} = \delta_{\text{UZ.WT}}(d) + \varepsilon_{\text{sol}}(T) + \varepsilon_{\text{EA}}(T, A, F)$$
 (12)

In Equation (12), ε_{EA} is the isotopic fractionation due to excess air at a given recharge temperature T, amount of initially entrapped air A, and modification F of that entrapped air due to partial

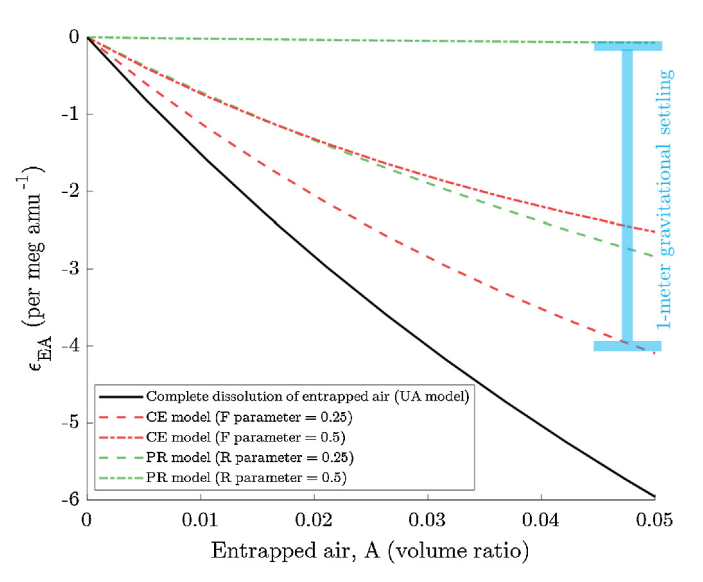


Fig. 8. Sensitivity of ε_{EA} to entrapped air amount for Xe isotopes in groundwater (i.e. δ^* Xe). Two common excess-air models (CE and PR models) and their shared limiting case of complete dissolution of entrapped air (i.e. the unfractionated excess air [UA] model: F=0, R=0) are considered. The F parameter in the CE model refers to the partiality of dissolution (the ratio of initial to final entrapped air to water volumetric ratios). The R parameter in the PR model refers to the degree of diffusive re-equilibration of supersaturated dissolved gases with the overlying unsaturated zone (such that higher R values indicate more complete re-equilibration). For comparison (blue scale), note that the fractionation due to 1 m of gravitational settling is \sim 4 per meg amu $^{-1}$.

dissolution or re-equilibration. Excess air can be added to ground-water and fractionated via either the closed-system equilibration (CE, Aeschbach-Hertig et al., 1999) or partial re-equilibration (PR, Stute et al., 1995) models. Reconstructing the isotopic composition of unsaturated-zone air $\delta_{\rm UZ,WT}$, at water-table depth d, requires knowledge of both $\varepsilon_{\rm sol}$ and $\varepsilon_{\rm EA}$ (Equation (12)). By measuring bulk noble gas concentrations in a given groundwater sample to determine T, A, and F, the $\varepsilon_{\rm sol}$ values determined in this study can be substituted directly into Equation (12).

However, to quantify ε_{FA} , an excess-air model (typically either the CE or PR model) and the values of $\varepsilon_{\rm sol}$ and/or $\varepsilon_{\rm kin}$ presented in this study must be used. In Fig. 8, we show that $\varepsilon_{\rm EA}$ is small in magnitude and largely insensitive to the choice of excess-air model, owing to the small values of ε_{sol} and ε_{kin} determined in this study. The range of A (the volumetric ratio of initially entrapped air to water) considered in Fig. 8 covers the range of realistic values in groundwater. For reference, assuming complete dissolution of entrapped air (i.e. the unfractionated-air [UA] model), A = 0 corresponds to 0% neon supersaturation, ΔNe , while A = 0.05 corresponds to $\Delta Ne = \sim 450\%$. As shown in Fig. 8, differences between ε_{EA} calculated via the PR and CE models for typical values of fractionation and re-equilibration parameters, F and R, are typically \sim 5 per meg amu $^{-1}$, equivalent to \sim 1 m of gravitational settling fractionation. Similar results (\sim 5–10 per meg amu⁻¹ CE vs. PR differences) were found for Kr isotopic fractionation due to excess air (Supplemental Fig. S13). We therefore suggest that dissolved δ^* Kr and δ^* Xe in groundwater represent promising new tracers of past water-table depth, based on our finding that ε_{EA} is small and rather insensitive to the choice of excess-air model.

5. Conclusions

In this study, we present results from a new method for highprecision measurement of Ar, Kr, and Xe stable isotope ratios in water. By conducting closed-system experiments at temperatures from \sim 2-20°C, we have determined freshwater Ar, Kr, and Xe isotopic solubility fractionation factors and their temperature dependences. We also carried out three separate air-water gas exchange experiments in which gas disequilibrium was induced by rapid cooling of water for the purpose of modeling kinetic fractionation due to diffusion in water. The solubility and kinetic fractionation factors we found exhibit mass proportionality for different isotope ratios of a given element and decrease in isotopic massdifference-normalized magnitude with increasing atomic number. The discovery of solubility and kinetic fractionation factors near unity for stable Kr and Xe isotopes gives promise to the potential for δ^* Kr and δ^* Xe in groundwater as a novel tool for the reconstruction of past water-table depths.

Acknowledgements

We are grateful to Ross Beaudette, Bill Paplawsky, and Adam Cox for assistance and advice on designing the laboratory infrastructure that enabled this research. We also thank Michael Bender, Roberta Hamme, Ray Weiss, Martin Stute, Justin Kulongoski, Steve Emerson, Kevin Tempest, and Sarah Shackleton for helpful discussions, suggestions, and equipment loans that contributed to the early development of this work. This study was supported by NSF award #1702704 as well as an NSF Graduate Research Fellowship. All data and relevant model code are accessible in the Supplementary materials.

Appendix A. Supplementary material

Supplementary material related to this article can be found online at https://doi.org/10.1016/j.epsl.2019.03.008.

References

- Aeschbach-Hertig, W., Peeters, F., Beyerle, U., Kipfer, R., 2000. Palaeotemperature reconstruction from noble gases in ground water taking into account equilibration with entrapped air. Nature 405, 1040–1044. https://doi.org/10.1038/35016542.
- Aeschbach-Hertig, W., Peeters, F., Beyerle, U., Kipfer, R., 1999. Interpretation of dissolved atmospheric noble gases in natural waters. Water Resour. Res. 35, 2779–2792. https://doi.org/10.1029/1999WR900130.

- Aeschbach-Hertig, W., Solomon, D.K., 2013. The noble gases as geochemical tracers. In: Burnard, P. (Ed.), The Noble Gases as Geochemical Tracers. Springer-Verlag, pp. 81–122.
- Benson, B.B., Krause, D., 1980. Isotopic fractionation of helium during solution: a probe for the liquid state. J. Solution Chem. 9, 895–909.
- Benson, B.B., Krause, D., 1984. The concentration and isotopic fractionation of oxygen dissolved in freshwater and seawater in equilibrium with the atmosphere determination of the Henry coefficient. Limnol. Oceanogr. 29, 620–632.
- Beyerle, U., Aeschbach-Hertig, W., Imboden, D.M., Baur, H., Graf, T., Kipfer, R., 2000.

 A mass, spectrometric system for the analysis of noble gases and tritium from water samples. Environ. Sci. Technol. 34, 2042–2050. https://doi.org/10.1021/es990840h
- Bourg, I.C., Sposito, G., 2008. Isotopic fractionation of noble gases by diffusion in liquid water: molecular dynamics simulations and hydrologic applications. Geochim. Cosmochim. Acta 72, 2237–2247. https://doi.org/10.1016/j.gca.2008. 02.012
- Clever, H.L. (Ed.), 1979. Krypton, Xenon, and Radon-Gas Solubilities, 1st ed. Pergamon, Tarrytown, N.Y.
- Grew, K.E., Ibbs, T.L., 1953. Thermal diffusion in gases. Q. J. R. Meteorol. Soc. 79, 458. https://doi.org/10.1002/qj.49707934127.
- Hamme, R.C., Emerson, S.R., 2004a. Measurement of dissolved neon by isotope dilution using a quadrupole mass spectrometer. Mar. Chem. 91, 53–64. https://doi.org/10.1016/J.MARCHEM.2004.05.001.
- Hamme, R.C., Emerson, S.R., 2004b. The solubility of neon, nitrogen and argon in distilled water and seawater. Deep-Sea Res., Part 1, Oceanogr. Res. Pap. 51, 1517–1528. https://doi.org/10.1016/j.dsr.2004.06.009.
- Hamme, R.C., Severinghaus, J.P., 2007. Trace gas disequilibria during deep-water formation. Deep-Sea Res., Part 1, Oceanogr. Res. Pap. 54, 939–950. https:// doi.org/10.1016/j.dsr.2007.03.008.
- Jähne, B., Heinz, G., Dietrich, W., 1987. Measurement of the diffusion coefficients of sparingly soluble gases in water. J. Geophys. Res. 92, 10767. https://doi.org/10. 1029/JC092iC10p10767.
- Jähne, B., Huber, W., Dutzi, A., Wais, T., Ilmberger, J., 1984. Wind/wave-tunnel experiment on the Schmidt number and wave field dependence of air/water gas exchange. In: Gas Transfer at Water Surfaces. Springer Netherlands, Dordrecht, pp. 303–309.
- Jenkins, W.J., Beg, M.A., Clarke, W.B., Wangersky, P.J., Craig, H., 1972. Excess ³He in the Atlantic Ocean. Earth Planet. Sci. Lett. 16, 122–126. https://doi.org/10.1016/ 0012-821X(72)90245-2
- Klots, C.E., Benson, B.B., 1963. Isotope effect in the solution of oxygen and nitrogen in distilled water. J. Chem. Phys. 38, 890–892. https://doi.org/10.1063/1.1733778.
- Knox, M., Quay, P.D., Wilbur, D., 1992. Kinetic isotopic fractionation during air-water gas transfer of O₂, N₂, CH₄, and H₂. J. Geophys. Res. 97, 20335. https://doi.org/ 10.1029/92IC00949.
- Ledwell, J.J., 1984. The variation of the gas transfer coefficient with molecular diffusity. In: Gas Transfer at Water Surfaces. Springer Netherlands, Dordrecht, pp. 293–302
- Lippmann, J., Stute, M., Torgersen, T., Moser, D.P., Hall, J.A., Lin, L., Borcsik, M., Bellamy, R.E.S., Onstott, T.C., 2003. Dating ultra-deep mine waters with noble gases and ³⁶Cl, Witwatersrand Basin, South Africa. Geochim. Cosmochim. Acta 67, 4597–4619. https://doi.org/10.1016/S0016-7037(03)00414-9.
- Loose, B., Jenkins, W.J., Moriarty, R., Brown, P., Jullion, L., Naveira Garabato, A.C., Torres Valdes, S., Hoppema, M., Ballentine, C., Meredith, M.P., 2016. Estimating the recharge properties of the deep ocean using noble gases and helium isotopes. J. Geophys. Res., Oceans 121, 5959–5979. https://doi.org/10.1002/2016JC011809.
- Mazor, E., 1972. Paleotemperatures and other hydrological parameters deduced from noble gases dissolved in groundwaters; Jordan Rift Valley, Israel. Geochim. Cosmochim. Acta 36, 1321–1336. https://doi.org/10.1016/0016-7037(72)90065-8.
- Muccitelli, J., Wen, W.-Y., 1978. Solubilities of hydrogen and deuterium gases in water and their isotope fractionation factor. J. Solution Chem. 7, 257–267. https://doi.org/10.1007/BF00644273.
- Nicholson, D., Emerson, S., Caillon, N., Jouzel, J., Hamme, R.C., 2010. Constraining ventilation during deepwater formation using deep ocean measurements of the dissolved gas ratios ⁴⁰Ar/³⁶Ar, N₂/Ar, and Kr/Ar. J. Geophys. Res. 115, C11015. https://doi.org/10.1029/2010JC006152.
- Orsi, A.J., 2013. Temperature Reconstruction at the West Antarctic Ice Sheet Divide, for the Last Millennium, from the Combination of Borehole Temperature and Inert Gas Isotope Measurements. Ph.D. thesis. University of California, San Diego.
- Seltzer, A.M., Severinghaus, J.P., Andraski, B.J., Stonestrom, D.A., 2017. Steady state fractionation of heavy noble gas isotopes in a deep unsaturated zone. Water Resour. Res. 53, 2716–2732. https://doi.org/10.1002/2016WR019655.
- Severinghaus, J.P., Bender, M.L., Keeling, R.F., Broecker, W.S., 1996. Fractionation of soil gases by diffusion of water vapor, gravitational settling, and thermal diffusion. Geochim. Cosmochim. Acta 60, 1005–1018. https://doi.org/10.1016/0016-7037(96)00011-7.
- Severinghaus, J.P., Grachev, A., Luz, B., Caillon, N., 2003. A method for precise measurement of argon 40/36 and krypton/argon ratios in trapped air in polar ice with applications to past firn thickness and abrupt climate change in Greenland and at Siple Dome, Antarctica. Geochim. Cosmochim. Acta 67, 325–343. https://doi.org/10.1016/S0016-7037/02)00965-1.

- Stanley, R.H., Baschek, B., Lott III, D.E., Jenkins, W.J., 2009. A new automated method for measuring noble gases and their isotopic ratios in water samples. Geochem. Geophys. Geosyst. 10, 5008. https://doi.org/10.1029/2009GC002429.
- Stanley, R.R., Jenkins, W., 2013. Noble gases in seawater as tracers for physical and biogeochemical ocean processes. In: The Noble Gases as Geochemical Tracers, pp. 55–79.
- Stute, M., Forster, M., Frischkorn, H., Serejo, A., Clark, J.F., Schlosser, P., Broecker, W.S., Bonani, G., 1995. Cooling of tropical Brazil (5C) during the Last Glacial maximum. Science 80 (269), 379–383. https://doi.org/10.1126/science.269.5222. 379.
- Tempest, K.E., Emerson, S., 2013. Kinetic isotopic fractionation of argon and neon during air-water gas transfer. Mar. Chem. 153, 39–47. https://doi.org/10.1016/j.marchem.2013.04.002.
- Torgersen, T., Clarke, W.B., 1985. Helium accumulation in groundwater, I: an evaluation of sources and the continental flux of crustal ⁴He in the Great Artesian

- Basin, Australia. Geochim. Cosmochim. Acta 49, 1211–1218. https://doi.org/10.1016/0016-7037(85)90011-0.
- Tyroller, L., Brennwald, M.S., Busemann, H., Maden, C., Baur, H., Kipfer, R., 2018. Negligible fractionation of Kr and Xe isotopes by molecular diffusion in water. Earth Planet. Sci. Lett. 492, 73–78. https://doi.org/10.1016/J.EPSL.2018.03.047.
- Tyroller, L., Brennwald, M.S., Mächler, L., Livingstone, D.M., Kipfer, R., 2014. Fractionation of Ne and Ar isotopes by molecular diffusion in water. Geochim. Cosmochim. Acta 136, 60–66. https://doi.org/10.1016/j.gca.2014.03.040.
- Wen, T., Castro, M.C., Nicot, J.-P., Hall, C.M., Larson, T., Mickler, P., Darvari, R., 2016. Methane sources and migration mechanisms in shallow groundwaters in Parker and Hood Counties, Texas—a heavy noble gas analysis. Environ. Sci. Technol. 50, 12012–12021. https://doi.org/10.1021/acs.est.6b01494.